Published in final edited form as:
Nat Med. 2008 March ; 14(3): 337. doi:10.1038/nm1715.

Differential regulation of central nervous system autoimmunity by T_H1 and T_H17 cells

Ingunn M Stromnes[1], **Lauren M Cerretti**[1], **Denny Liggitt**[2], **Robert A Harris**[3], and **Joan M Goverman**[1]

[1]Department of Immunology, Box 357650, HSC H474B, 1959 NE Pacific Street, Seattle, Washington 98195, USA.

[2]Department of Comparative Medicine, Box 357190, University of Washington, 1959 NE Pacific Street, Seattle, Washington 98195, USA.

[3]Applied Immunology Group, Department of Clinical Neurosciences, Karolinska Institute, Solna, CMM, L8:04, 171 76 Stockholm, Sweden.

Abstract

Multiple sclerosis is an inflammatory, demyelinating disease of the central nervous system (CNS) characterized by a wide range of clinical signs[1]. The location of lesions in the CNS is variable and is a crucial determinant of clinical outcome. Multiple sclerosis is believed to be mediated by myelin-specific T cells, but the mechanisms that determine where T cells initiate inflammation are unknown. Differences in lesion distribution have been linked to the HLA complex, suggesting that T cell specificity influences sites of inflammation2. We demonstrate that T cells that are specific for different myelin epitopes generate populations characterized by different T helper type 17 (T_H17) to T helper type 1 (T_H1) ratios depending on the functional avidity of interactions between TCR and peptide-MHC complexes. Notably, the T_H17:T_H1 ratio of infiltrating T cells determines where inflammation occurs in the CNS. Myelin-specific T cells infiltrate the meninges throughout the CNS, regardless of the T_H17:T_H1 ratio. However, T cell infiltration and inflammation in the brain parenchyma occurs only when T_H17 cells outnumber T_H1 cells and trigger a disproportionate increase in interleukin-17 expression in the brain. In contrast, T cells showing a wide range of T_H17:T_H1 ratios induce spinal cord parenchymal inflammation. These findings reveal critical differences in the regulation of inflammation in the brain and spinal cord.

Experimental autoimmune encephalomyelitis (EAE) is an animal model that shows many similarities to multiple sclerosis3. However, rodent EAE differs from multiple sclerosis by manifesting as ascending flaccid paralysis, reflecting unexplained preferential targeting of inflammation to the spinal cord (described as classic EAE). In a small number of antigen-specific models, brain inflammation occurs (described as atypical EAE)4–8. Interferon-γ (IFN-γ) deficiency also causes certain myelin-specific T cells to preferentially induce brain

Correspondence should be addressed to J.M.G. (goverman@u.washington.edu).

Note: Supplementary information is available on the Nature Medicine website.

AUTHOR CONTRIBUTIONS

I.M.S. conducted most of the experiments; L.M.C. assisted with the RT-PCR experiments and data analyses; D.L. assisted with the evaluation of the histochemical analyses; R.A.H. provided rMOG production protocol and helpful discussions; I.M.S. and J.M.G. designed the study, analyzed the data and wrote the manuscript; and J.M.G. secured the funding.

Published online at http://www.nature.com/naturemedicine Reprints and permissions information is available online at http://npg.nature.com/reprintsandpermissions

inflammation9,10. These studies raise the possibility that specific sites of inflammation in the CNS may reflect T cell specificity, as well as the ability to produce IFN-γ. T_H1 cells secreting IFN-γ were considered to be the primary mediators of EAE, but recent studies suggest that T_H17 cells show greater pathogenicity[11]. The roles of major histocompatibility complex (MHC) haplotype, T cell specificity and effector function in determining where inflammation occurs in the CNS are not well understood.

We investigated how the MHC locus influences CNS inflammation in MHC congenic C3H mice. C3H.SW (H-2^b) mice that were immunized with recombinant rat myelin oligodendrocyte glycoprotein (rMOG) showed classic EAE, as described[12]. To our surprise, C3HeB/Fej (H-2^k) mice suffered from severe, atypical EAE that was characterized by proprioception defects, ataxia, spasticity and hyper-reflexivity (Fig. 1a). Inflammatory cells infiltrated the spinal cord and optic nerve of both strains. However, inflammation in C3H.SW brains was primarily restricted to meninges, ventricles and vessels, whereas C3HeB/Fej brains were characterized by severe parenchymal infiltration of $CD4^+$ T cells, macrophages and activated microglia (Fig. 1b). Lesions in the cerebellar and periventricular white matter, brain stem, pons, fimbria hippocampi and cortex were consistently observed. The numbers of $CD4^+$, $CD8^+$, $B220^+$, Gr-1^+, $CD11c^+$ and $F4/80^+$ cells were similar in the spinal cords of both strains, but were increased in C3HeB/Fej compared with C3H.SW brains (data not shown).

The gene encoding MOG lies in the MHC locus; however, no differences were found in its sequence or expression between C3H.SW and C3HeB/Fej mice (Supplementary Fig. 1 online). We therefore investigated the role of lymphocyte subsets in inducing brain inflammation in C3HeB/Fej mice, as their activity is MHC-allele dependent. rMOG-induced EAE in C3HeB/Fej B cell–deficient (μ $MT^{-/-}$), $CD8^+$ T cell–deficient ($B2m^{-/-}$) and CD8-depleted mice showed the same brain inflammation as wild-type mice. In contrast, EAE was completely abrogated by depleting $CD4^+$ T cells (Supplementary Fig. 1 and Supplementary Table 1 online), demonstrating that $CD4^+$ T cells are necessary and sufficient to induce brain inflammation.

Two $CD4^+$ T cell epitopes, $MOG_{79–90}$ and $MOG_{97–114}$, presented by I-E^k and I-A^k, respectively, were identified in C3HeB/Fej mice (Supplementary Fig. 2 online). C3H.SW $CD4^+$ T cells respond only to $MOG_{35–55}$ (ref. [12] and Supplementary Fig. 2). To compare the encephalitogenic activities of epitope-specific T cells and eliminate any other genetic influences, we restimulated T cells from rMOG-immunized C3HeB/Fej × C3H.SW (F1) mice with different peptides and transferred them separately into F1 recipients. $MOG_{35–55}$- and $MOG_{79–90}$-specific T cells induced only spinal cord inflammation that resulted in classic EAE, whereas $MOG_{97–114}$-specific T cells induced brain, rather than spinal cord, inflammation that caused atypical EAE (Fig. 2a,b). However, we detected no differences in either the processing of rMOG by brain versus spinal cord antigen-presenting cells (APCs) (Supplementary Fig. 3 online) or the cell-surface expression of ESL-1, PSGL-1, LFA-1, VLA-4, CCR3, CCR5, CCR6, CCR9, CXCR3, CXCR4 and CXCR5 on epitope-specific T cells before transfer (data not shown).

To determine whether the effector function of $MOG_{97–114}$-specific T cells differed from that of $MOG_{79–90}$- or $MOG_{35–55}$-specific T cells, we analyzed the number of epitope-specific T_H17 and T_H1 cells in mice with rMOG-induced EAE. The T_H17:T_H1 ratio was significantly higher for $MOG_{97–114}$-specific T cells compared with the other specificities in spleen ($P < 0.005$) and CNS ($P < 0.0005$), owing to the fact that there were more IFN-γ^+ $MOG_{79–90}$-specific T cells and fewer interleukin-17 (IL-17)$^+$ $MOG_{35–55}$-specific T cells when compared with $MOG_{97–114}$-specific T cells (Supplementary Fig. 4 online). We investigated the influence of the T_H17:T_H1 ratio on lesion distribution in the CNS by adoptive transfer of rMOG-primed T cells that were skewed toward a T_H17 or T_H1 phenotype. Notably, $MOG_{35–55}$- and

$MOG_{79–90}$-specific T cells that were skewed toward a T_H17 phenotype now induced predominantly atypical EAE, and $MOG_{97–114}$-specific T cells that were skewed toward a T_H1 phenotype induced predominantly classic EAE (Fig. 2c), indicating that T cell effector function influences the sites of inflammation. Consistent with the clinical presentation, T_H17-biased T cells recruited more inflammatory cells to the brain than were recruited by T_H1-biased T cells (Fig. 2d,e).

To our surprise, despite preferential recruitment of inflammatory cells to the brain by T_H17-biased T cells, we did not observe preferential localization of the antigen-specific T_H17 cells themselves to the brain or spinal cord (Fig. 3a). Furthermore, there was substantial overlap in the number of T_H17 cells in the brains of $MOG_{97–114}$- and $MOG_{35–55}$-specific T cell recipients with atypical EAE compared with classic EAE (Fig. 3b), indicating that brain inflammation is not simply triggered by an increase in the absolute number of infiltrating antigen-specific T_H17 cells. Double-positive (IL-17^+IFN-γ^+) T cells were not detected (<1%) in the CNS at disease onset (data not shown). However, a comparison of the T_H17:T_H1 ratios in the brain and spinal cord of recipients with atypical versus classic EAE revealed that all three T cell specificities induced atypical EAE only when the T_H17:T_H1 ratio in the brain was ≥1. Conversely, classic EAE occurred when the T_H17:T_H1 ratio in the brain was ≤1 (Fig. 3c). Together, these data indicate that the T_H17:T_H1 ratio in the brain, rather than the absolute number of T_H17 cells, is the key parameter for determining whether inflammation occurs in the brain. Because the antigen-specific T_H1 cell number was significantly higher in the spinal cord compared with the brain in IL-12–skewed recipients ($P < 0.005$; Fig. 3a), we investigated whether the T_H17:T_H1 ratio also influences spinal cord inflammation. The range of T_H17:T_H1 ratios was the same for atypical EAE mice with and without tail paralysis, indicating that the ratio did not regulate spinal cord inflammation (Supplementary Fig. 5 online).

Because comparable numbers of antigen-specific T cells were detected in the brains of mice with classic and atypical EAE, we carried out immunohistochemical analyses to determine where T cells localized in the brain in the absence of inflammation. $CD4^+$ T cells were largely confined to the meninges in the brain in classic EAE, even though they extensively infiltrated the spinal cord parenchyma of same mice (Supplementary Fig. 5), in stark contrast to the parenchymal infiltration of the brain by $CD4^+$ T cells in atypical EAE (Fig. 2d). These data suggest that a predominance of T_H1 cells exerts an inhibitory influence in the brain at the stage of parenchymal infiltration.

To investigate the mechanism by which the T_H17:T_H1 ratio regulates inflammation in the brain, we analyzed the expression of inflammatory genes in the brains and spinal cords of healthy mice and recipients of T_H1- or T_H17-biased $MOG_{97–114}$ T cells showing either classic or atypical EAE. We observed no difference in IL-17Ra expression, but IFN-γRb expression was approximately fivefold higher in the brain compared with the spinal cord in healthy mice, suggesting that resident brain cells may be more responsive to IFN-γ than spinal cord cells (data not shown). However, we did not observe increased expression of genes associated with known mechanisms of IFN-γ– mediated suppression of EAE in the brains of mice with classic EAE. IL-27 (ref. 13), iNOS14, PD-1 (ref. 15), FAS16,17, FASL17, IL1-Ra18, IL-23 (ref. 19) and IL-23R20 transcripts were expressed at either equivalent levels in atypical and classic EAE brains or were expressed at higher levels in atypical EAE brains (Supplementary Table 2 online and data not shown). Furthermore, both Foxp3 and CD25 were induced only in atypical EAE brains (Supplementary Table 2), indicating that T_H1 cells do not suppress inflammation in the brain by preferentially recruiting regulatory T cells. We found it interesting that some genes were induced comparably in the brains of mice with both atypical and classic EAE, demonstrating that T cell infiltration in the meninges induces some responses in classic EAE brains despite the lack of parenchymal inflammation. Notably, the expression of several genes was strongly increased in a brain-specific manner in atypical EAE. The expression of IL-17,

CCL24, CCL11, CCL6 and MMP-12 was increased between five- and 26-fold in atypical compared with classic EAE brains, but differed no more than 2.5-fold in the spinal cords of both types of recipients (Supplementary Table 2).

IL-17 expression was particularly intriguing because it increased 25-fold in the brain compared with the spinal cord of mice with atypical EAE, but increased only 2.4-fold in the brain compared with the spinal cord in classic EAE mice. To determine whether the disproportionate increase in IL-17 expression in the brain in atypical EAE is responsible for triggering inflammation, we induced EAE by adoptively transferring T_H17-biased T cells and administering either neutralizing soluble IL-17 receptor or control IgG to the recipients. Although both groups had a 100% incidence of EAE, 8 out of 10 mice that received the IL-17–neutralizing reagent developed only classic EAE, and 9 out of 10 mice that received control IgG developed atypical EAE (Fig. 3d,e). Consistent with the clinical phenotype, neutralization of IL-17 eliminated parenchymal inflammation in the brain, but not spinal cord, at EAE onset (Fig. 3f). Neutralization of IL-17 reduced infiltration of neutrophils, but not $CD4^+$ T cells or $F4/80^+$ cells, in the spinal cord of mice with classic EAE (data not shown). Thus, enhanced IL-17 activity that occurs when T_H1 cells are not predominant in the infiltrating T cell population is required to trigger parenchymal inflammation in the brain, but not in the spinal cord.

The unique ability of non-skewed $MOG_{97–114}$-specific T cells to induce brain inflammation suggested that $MOG_{97–114}$-specific T cells intrinsically generate a higher T_H17:T_H1 ratio than the other specificities. Accordingly, the T_H17:T_H1 ratio for $MOG_{97–114}$-specific T cells was significantly higher than that of the other specificities directly after immunization with rMOG, even though all T cells were primed under the same conditions *in vivo* ($P < 0.05$; Fig. 4a). $MOG_{97–114}$-specific T cells also showed a significantly higher functional avidity for their cognate antigen compared with $MOG_{35–55}$- and $MOG_{79–90}$-specific T cells ($P < 0.005$; Fig. 4b), suggesting that the T_H17:T_H1 ratio may be influenced by functional avidity. This hypothesis was tested using T cells that were specific for myelin basic protein (MBP), $MBP_{Ac1–11}$, whose functional avidity for an analog peptide ($MBP_{Ac1–11Met4Lys8}$) is increased approximately 1,000-fold compared with $MBP_{Ac1–11}$ because of the increased affinity of the analog peptide for $I\text{-}A^u$ (Fig. 4c). T cells primed *in vivo* with the high avidity $MBP_{Ac1–11Met4Lys8}$ peptide showed significantly higher T_H17:T_H1 ratios than the same T cells primed with $MBP_{Ac1–11}$ ($P < 0.005$; Fig. 4d). Because the myelin-specific T cells were primed under identical conditions, with the cytokine milieu being the same, these results indicate that T cell functional avidity for pMHC is an independent determinant of T_H17:T_H1 ratios.

Together our studies indicate that the T_H17:T_H1 ratio of infiltrating myelin-specific T cells, which is determined in part by epitope-specific T cell functional avidity, is a critical determinant of brain, but not of spinal cord, inflammation. T cells showing both high and low T_H17:T_H1 ratios initially infiltrate the brain and spinal cord meninges. However, at low T_H17:T_H1 ratios, T cell infiltration proceeded into the spinal cord, but not brain, parenchyma. Our data identify differential production of IL-17 in the brain when T cells are reactivated at high versus low T_H17:T_H1 ratios as the mechanism regulating infiltration into the brain parenchyma. We established a critical role for IL-17 in the differential regulation of inflammation in the brain versus spinal cord by neutralizing IL-17 activity *in vivo*, which resulted in the loss of recruitment of inflammatory cells specifically to the brain parenchyma. Many of the genes showing a disproportionate increase in expression specifically in atypical EAE brains are consistent with the notion that enhanced local production of IL-17 in the brain triggers inflammation. IL-17 induces MMP-3 (ref. 21), accounting for the large increase in MMP-3 expression that we observed in atypical EAE brains. Neutrophils recruited by enhanced IL-17 activity import proteases and inactive pro-forms of MMP-8 and MMP-9 stored in their granules. MMP-3 activates latent MMP-8 and MMP-9 (ref. 22), which then contribute to blood

brain–barrier breakdown22,23 and enhance further neutrophil recruitment via cleavage of ELR chemokines24. CCL6 and CCL9, which were induced four- to fivefold in atypical versus classic EAE brains, are converted by neutrophil protease activity to potent attractants of macrophages and monocytes[25], leading to sustained myelin and axonal damage. MMP-12 expression, attributed primarily to macrophages in EAE[26], was also disproportionately increased in atypical versus classic EAE brains compared with spinal cords, consistent with the lack of recruitment of macrophages to the brain in classic EAE. Together, these findings imply that therapies targeting IL-17 activity may be most beneficial for patients with lesions in the brain and less effective for patients with lesions restricted primarily to the spinal cord.

METHODS

Mice

C3HeB/Fej, C3.SW-*H-2*^{b}/SnJ (C3H.SW), C3.129P2(B6)-*B2m*^{tm1Unc}/Dcr, B6.129S2-*Igh-6*^{tm1Cgn}/J, B10.PL(73 NS)/Sn, and C3H/Hej mice were purchased from the Jackson Laboratory and maintained in a specific pathogen–free facility at the University of Washington. $MBP_{Ac1–11}$ T cell receptor (TCR) transgenic mice were previously described[27]. We backcrossed the B6.129S2-*Igh-6*^{tm1Cgn}/J mutation onto the C3HeB/Fej and C3H.SWbackground for 10–12 generations. The University of Washington Institutional Animal Care and Use Committee approved all procedures.

Proteins and peptides

We produced rMOG (rat $MOG_{1–125}$) protein in *Escherichia coli* as described[28]. MOG peptides 35–55, 79–90, 97–114 (rat sequences) and $MBP_{Ac1–11}$ (mouse sequence) were synthesized by Genemed, and $MBP_{Ac1–11Met4Lys8}$ was synthesized at the California Institute of Technology, using Fmoc/HBTU chemistry. Peptides were purified to 99% purity.

EAE induction

We induced active EAE using 100 μg of rMOG and 200 ng of pertussis toxin (List Biological Laboratories) as described[29]. We induced passive EAE by culturing splenocytes (1×10^7 cells per ml) from rMOG-immunized mice for 3 d with either rMOG (25 μg ml^{-1}) or MOG peptides (10 μM for $MOG_{79–90}$ and $MOG_{97–114}$, 20 μM for $MOG_{35–55}$). We included 10 ng ml^{-1} of rIL-23 or rIL-12 (eBioscience) to skew cells toward a T_H17 or T_H1 phenotype, respectively, and intraperitoneally injected viable cells (2×10^7 cells per mouse) into sublethally irradiated (250 rad) mice. We scored the severity of classic EAE as: grade 1, paralyzed tail; grade 2, ataxic; grade 2.5, one hind leg paralyzed; grade 3, both hind legs paralyzed; grade 3.5, 3 legs paralyzed; grade 4, complete paralysis; grade 5, moribund; and the severity of atypical EAE as: grade 1, tail paralysis, hunched appearance; grade 2, ataxia, scruffy coat; grade 3, head tilt, hypersensitivity, spasticity or knuckling; grade 4, severe proprioception defects; grade 5, moribund.

Immunohistochemistry

We stained 7-μm frozen sagittal sections from perfused CNS tissue for CD4 (L3T4, BD Biosciences) and F4/80 (BM8, Invitrogen), and used either IgG-biotin (BD Biosciences), Vectastain (Vector) and 3,3′-diaminobenzidine tetrahydrochloride (Sigma), or sAv-488 and rat 546-specific antibody (Molecular Probes) for detection. DAPI was included in some experiments to detect nuclei. For image analyses, we stained four sections per mouse, encompassing the spinal cord (lumbar, thoracic and cervical) and brain (brain stem, cerebellum, peri-ventricular region, cortex and olfactory bulb), for F4/80 and photographed lesions at 10× using PixelLink digital-camera software. We analyzed the percent F4/80^{+} using IP Lab (Scanalytics). Because specific CNS regions targeted by inflammation varied in individual

mice, we summed the percent $F4/80^+$ for the three spinal cord regions and the five brain regions, and show averaged results for the recipients of each T cell specificity ± s.d.

Flow cytometry

We stained CNS mononuclear cells from perfused mice at EAE onset as described[30], and carried out intracellular cytokine staining according to manufacturer's directions (BD Biosciences). We used antibodies to CD4 (L3T4), CD11c (HL3), Gr-1/Ly6G (1A8), IFN-γ–FITC (XMG.1.2), IL-17–PE (TC11-18H10), CXCR5 (2G8) and CXCR4 (2B11) from BD Biosciences, F4/80 (RM2915) from Caltag, and CXCR3 (220803) and CCR9 (242503) from R&D Systems. Mouse chemokine–human IgG3 fusion proteins CCL19, CCL20, CCL22, and P- and E-selectin–human IgM fusion proteins were a gift from D. Campbell (Benaroya Research Institute) and were detected using human IgG–specific or human IgM–specific antibodies (Jackson ImmunoResearch).

Enzyme-linked immunosorbent spot

We plated splenocytes (2×10^5 or 1×10^6 cells per well) or brain or spinal cord mononuclear cells from perfused mice (typically between $1–10 \times 10^5$ cells per well) in duplicate in multiscreen nitrocellulose 96-well Enzyme-linked immunosorbent spot (ELISPOT) plates (Millipore) and carried out ELISPOT assays according to BD Biosciences protocols. IFN-γ–specific antibody pairs, IL-17–specific (TC11-18H10) and biotinylated IL-17–specific (TC11-8H4.1) antibodies were from BD Biosciences. We subtracted background spots without antigen (<10 spots per well) from the total number of spots with antigen.

IL-17 neutralization

We adoptively transferred IL-23–skewed $MOG_{97–114}$ T cells and administered either 100 μg soluble mouse IL-17RA–Fc protein (generous gift from ZymoGenetics) or purified mouse IgG (Jackson Immuno Research) by intraperitoneal injection on day 0 and every other day for 7 d.

Functional avidity

We incubated 1×10^6 spleen and lymph node cells from rMOG-immunized mice with MOG peptides for 16–18 h, and detected responses by IFN-γ and IL-17 ELISPOT. We determined the peptide dose eliciting 50% maximum response using the software program R (http://www.r-project.org) and the dose-response curve function. For MBP-specific T cells, we incubated splenocytes from $MBP_{Ac1–11}$–specific TCR transgenic mice with titrating doses of $MBP_{Ac1–11}$ or $MBP_{Ac1–11Met4Lys8}$ for 48 h and pulsed the cultures with 1 μCi $[^3H]$ thymidine for 16–18 h.

T_H17:T_H1 ratio for MBP epitopes

We subcutaneously immunized B10.PL(73 NS)/Sn $H\text{-}2^u$ mice with 200 μg of $MBP_{Ac1–11}$ or $MBP_{Ac1–11Met4Lys8}$ in CFA and restimulated splenocytes (1×10^6 cells per well) from immunized mice with peptide 7 d later. We determined the number of IL-17 and IFN-γ–secreting cells by ELISPOT.

Statistics

We derived *P* values for Figure 2b,e; Figure 3a,c,d; and Figure 4a,d using two-tailed Student's *t* tests, and carried out χ-square test in Figure 2c and Figure 3c. ANOVA was used in Figure 4b ($\alpha = 0.05$).

Supplementary Material

Refer to Web version on PubMed Central for supplementary material.

Acknowledgments

We thank S. Levin at ZymoGenetics, Inc. for the IL17RA-Fc protein, H. Simkins and N. Mausolf for technical support and animal husbandry, D. Goverman, L. Kicknosway and R. Rowe for assistance with immunohistochemistry, R. Ransohoff for helpful discussions, T. Brabb, L. Castelli, Q. Ji, H. Simkins and A. Weinmann for critical reading of the manuscript, and B. Teeple for assistance with statistical analyses. This work was supported by the National Multiple Sclerosis Society (RG 3851-A-5 to J.M.G.) and the US National Institutes of Health (AI072737 to J.M.G.) and Public Health Service (T32-CA009537 to I.M.S.).

References

1. Sospedra M, Martin R. Immunology of multiple sclerosis. Annu. Rev. Immunol 2005;23:683–747. [PubMed: 15771584]
2. Fukazawa T, et al. Both the HLA-CPB1 and -DRB1 alleles correlate with risk for multiple sclerosis in Japanese: clinical phenotypes and gender as important factors. Tissue Antigens 2000;55:199–205. [PubMed: 10777094]
3. Raine, C. The lesion in multiple sclerosis and chronic relapsing experimental allergic encephalomyelitis: a structural comparison. In: Raine, CS.; McFarland, HF.; Tourtellotte, WW., editors. Multiple Sclerosis: Clinical and Pathogenetic Basis. London: Chapman and Hall; 1997. p. 243-286.
4. Storch MK, et al. Autoimmunity to myelin oligodendrocyte glycoprotein in rats mimics the spectrum of multiple sclerosis pathology. Brain Pathol 1998;8:681–694. [PubMed: 9804377]
5. Tsunoda I, Kuang LQ, Theil DJ, Fujinami RS. Antibody association with a novel model for primary progressive multiple sclerosis: induction of relapsing-remitting and progressive forms of EAE in H2s mouse strains. Brain Pathol 2000;10:402–418. [PubMed: 10885659]
6. Muller DM, Pender MP, Greer JM. A neuropathological analysis of experimental autoimmune encephalomyelitis with predominant brain stem and cerebellar involvement and differences between active and passive induction. Acta Neuropathol 2000;100:174–182. [PubMed: 10963365]
7. Weissert R, et al. MHC class II-regulated central nervous system autoaggression and T cell responses in peripheral lymphoid tissues are dissociated in myelin oligodendrocyte glycoprotein–induced experimental autoimmune encephalomyelitis. J. Immunol 2001;166:7588–7599. [PubMed: 11390515]
8. Kjellen P, et al. The H2-Ab gene influences the severity of experimental allergic encephalomyelitis induced by proteolipoprotein peptide 103–116. J. Neuroimmunol 2001;120:25–33. [PubMed: 11694316]
9. Wensky AK, et al. IFN-gamma determines distinct clinical outcomes in autoimmune encephalomyelitis. J. Immunol 2005;174:1416–1423. [PubMed: 15661899]
10. Abromson-Leeman S, et al. T cell properties determine disease site, clinical presentation and cellular pathology of experimental autoimmune encephalomyelitis. Am. J. Pathol 2004;165:1519–1533. [PubMed: 15509523]
11. Steinman L. A brief history of T_H17, the first major revision in the T_H1/T_H2 hypothesis of T cell–mediated tissue damage. Nat. Med 2007;13:139–145. [PubMed: 17290272]
12. Mendel I, Kerlero de Rosbo N, Ben-Nun A. A myelin oligodendrocyte glycoprotein peptide induces typical chronic experimental autoimmune encephalomyelitis in H-2b mice: fine specificity and T cell receptor Vβ expression of encephalitogenic T cells. Eur. J. Immunol 1995;25:1951–1959. [PubMed: 7621871]
13. Fitzgerald DC, et al. Suppressive effect of IL-27 on encephalitogenic T_H17 cells and the effector phase of experimental autoimmune encephalomyelitis. J. Immunol 2007;179:3268–3275. [PubMed: 17709543]
14. van der Veen RC. Nitric oxide and T helper cell immunity. Int. Immunopharmacol 2001;1:1491–1500. [PubMed: 11515814]
15. Cheng X, et al. The PD-1/PD-L pathway is up-regulated during IL-12–induced suppression of EAE mediated by IFN-γ. J. Neuroimmunol 2007;185:75–86. [PubMed: 17320975]

16. Spanaus KS, Schlapbach R, Fontana A. TNF-α and IFN-γ render microglia sensitive to Fas ligand–induced apoptosis by induction of Fas expression and down-regulation of Bcl-2 and Bcl-xL. Eur. J. Immunol 1998;28:4398–4408. [PubMed: 9862377]

17. Badie B, Schartner J, Vorpahl J, Preston K. Interferon-γ induces apoptosis and augments the expression of Fas and Fas ligand by microglia *in vitro*. Exp. Neurol 2000;162:290–296. [PubMed: 10739635]

18. Muhl H, Pfeilschifter J. Anti-inflammatory properties of pro-inflammatory interferon-γ. Int. Immunopharmacol 2003;3:1247–1255. [PubMed: 12890422]

19. Cruz A, et al. Cutting edge: IFN-γ regulates the induction and expansion of IL-17–producing CD4 T cells during mycobacterial infection. J. Immunol 2006;177:1416–1420. [PubMed: 16849446]

20. Harrington LE, et al. Interleukin 17–producing CD4· effector T cells develop via a lineage distinct from the T helper type 1 and 2 lineages. Nat. Immunol 2005;6:1123–1132. [PubMed: 16200070]

21. Park H, et al. A distinct lineage of CD4 T cells regulates tissue inflammation by producing interleukin 17. Nat. Immunol 2005;6:1133–1141. [PubMed: 16200068]

22. Yong VW, Power C, Forsyth P, Edwards DR. Metalloproteinases in biology and pathology of the nervous system. Nat. Rev. Neurosci 2001;2:502–511. [PubMed: 11433375]

23. Agrawal S, et al. Dystroglycan is selectively cleaved at the parenchymal basement membrane at sites of leukocyte extravasation in experimental autoimmune encephalomyelitis. J. Exp. Med 2006;203:1007–1019. [PubMed: 16585265]

24. Tester AM, et al. LPS responsiveness and neutrophil chemotaxis *in vivo* require PMN MMP-8 activity. PLoS ONE 2007;2:e312. [PubMed: 17375198]

25. Berahovich RD, et al. Proteolytic activation of alternative CCR1 ligands in inflammation. J. Immunol 2005;174:7341–7351. [PubMed: 15905581]

26. Toft-Hansen H, Nuttall RK, Edwards DR, Owens T. Key metalloproteinases are expressed by specific cell types in experimental autoimmune encephalomyelitis. J. Immunol 2004;173:5209–5218. [PubMed: 15470066]

27. Goverman J, et al. Transgenic mice that express a myelin basic protein–specific T cell receptor develop spontaneous autoimmunity. Cell 1993;72:551–560. [PubMed: 7679952]

28. Abdul-Majid KB, et al. Screening of several H-2 congenic mouse strains identified H-2(q) mice as highly susceptible to MOG-induced EAE with minimal adjuvant requirement. J. Neuroimmunol 2000;111:23–33. [PubMed: 11063818]

29. Stromnes IM, Goverman JM. Active induction of experimental allergic encephalomyelitis. Nature Protocols 2006;1:1810–1819.

30. Brabb T, et al. *In situ* tolerance within the central nervous system as a mechanism for preventing autoimmunity. J. Exp. Med 2000;192:871–880. [PubMed: 10993917]

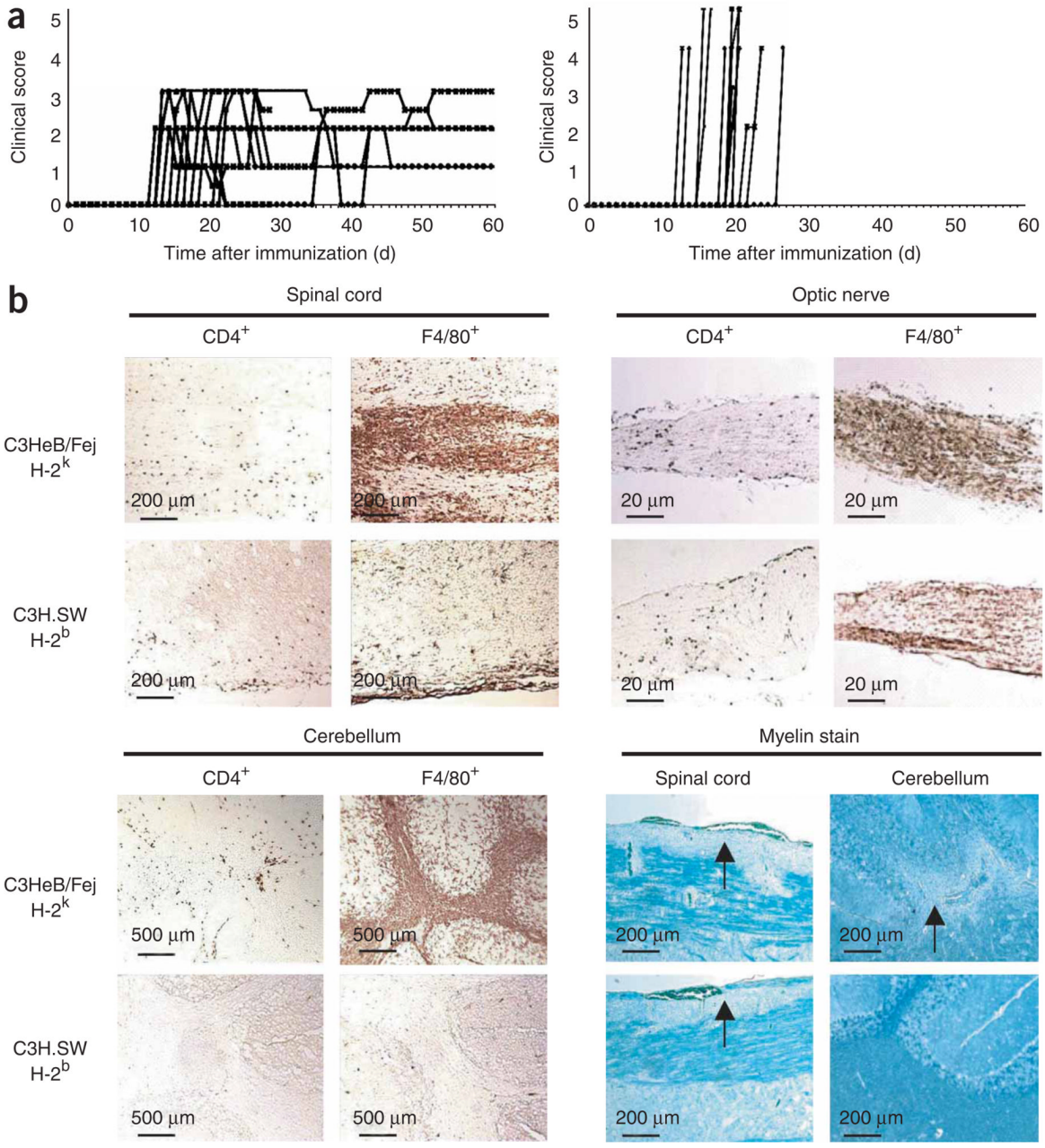

Figure 1.

CNS autoimmunity differs in C3H MHC congenic mice. (**a**) Clinical course of EAE in C3H.SW (left, $n = 11$) and C3HeB/Fej (right, $n = 13$) mice. C3H.SW mice were scored according to a classic EAE scale and C3HeB/Fej mice were scored using an atypical EAE scale. Results are representative of two experiments. (**b**) Immunopathology of CNS tissues from mice killed at onset of EAE. Immunochemically stained $CD4^+$ and $F4/80^+$ cells were detected as brown foci. Pale-staining regions of Luxol-Fast Blue–stained sections demonstrate areas of myelin loss (arrows).

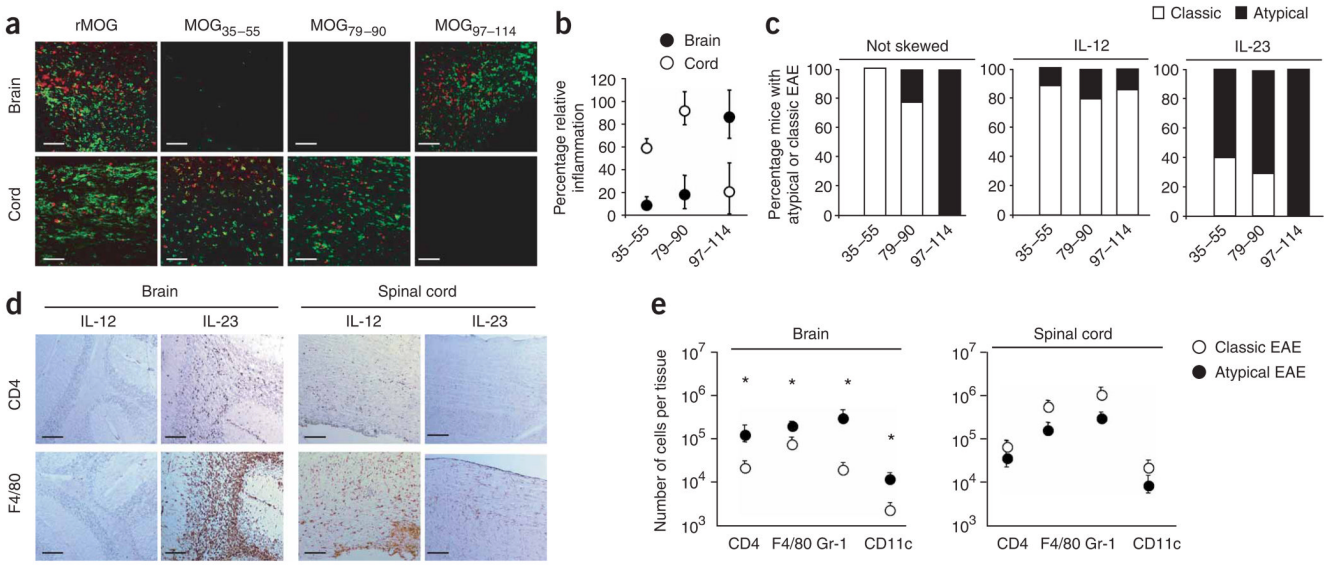

Figure 2.

T cell skewing toward a T_H17 or T_H1 phenotype directs inflammation to the brain or spinal cord. (**a**) Representative CD4 (red) and F4/80 (green) staining of cerebellum and lumbar spinal cord sections of F1 recipients of epitope-specific T cells (the atypical:classic EAE ratios were rMOG, 3:0; $MOG_{35–55}$, 0:6; $MOG_{79–90}$, 2:7; $MOG_{97–114}$, 11:0). Scale bar, 200 μm. (**b**) The distribution of inflammation between brain and spinal cord, as quantified by image analysis software, was significantly different for all specificities ($P < 0.0001$). Error bars indicate s.d. (**c**) Percentage of F1 recipients showing atypical or classic EAE after transfer of T cells cultured with either peptide alone, peptide and IL-12, or peptide and IL-23 (n = 5–11 recipients per group). Some IL-23–skewed T cell recipients with atypical EAE also showed tail paralysis (3/10, 2/5 and 4/6 for $MOG_{97–114}$-, $MOG_{79–90}$- and $MOG_{35–55}$-specific T cells, respectively). Atypical EAE incidence was significantly higher for non-skewed $MOG_{97–114}$- compared with $MOG_{79–90}$- ($P = 0.0001$) and $MOG_{35–55}$-specific T cells ($P = 0.0003$). The difference in disease phenotype induced by IL-23– and IL-12–skewed cells was significant ($P = 7.7 \times 10^{-19}$). (**d**) Immunohistochemical staining for $CD4^+$ and $F4/80^+$ cells in representative brain and spinal cord sections from IL-12– or IL-23–skewed $MOG_{97–114}$-specific T cell recipients. Scale bar, 200 μm. (**e**) Flow cytometric analyses of recipients in **c** revealed significantly more $CD4^+$, $F4/80^+$, Gr-1^+ and $CD11c^+$ cells in the brains of atypical compared with classic EAE mice ($P \leq 0.04$). Error bars represent s.e.m.

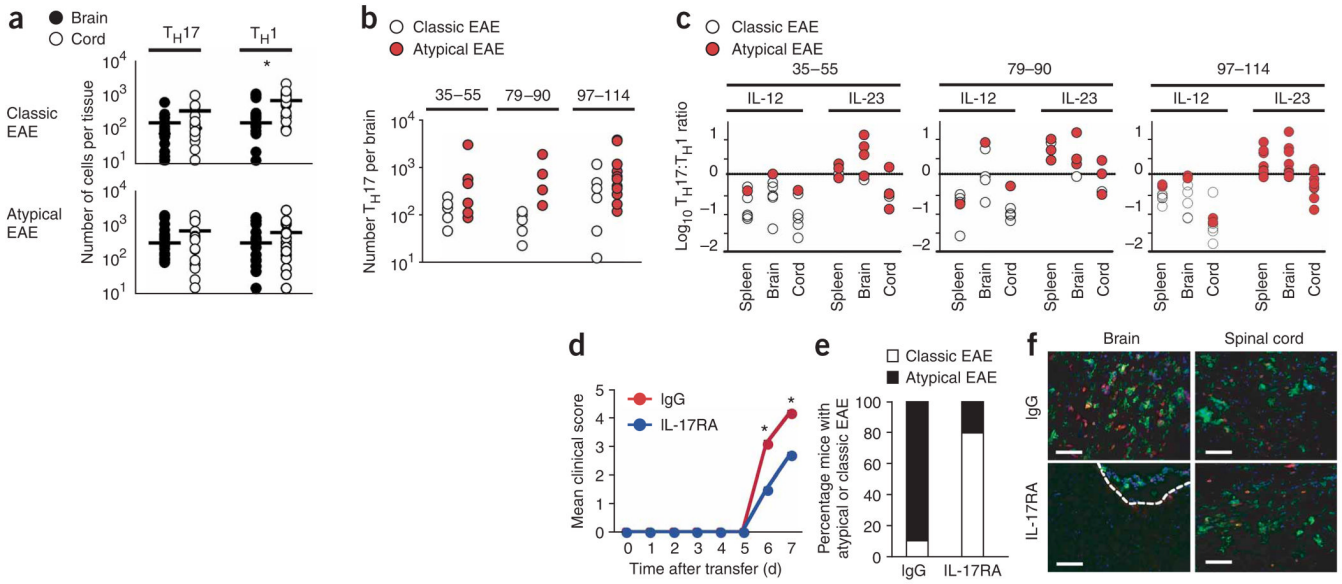

Figure 3.

IL-17 activity triggered by high T_H17:T_H1 ratios in the brain is required for parenchymal brain inflammation. (**a**) The numbers of MOG-specific T_H17 and T_H1 cells in brain and spinal cord of F1 recipients with atypical or classic EAE determined at disease onset by ELISPOT. Each circle represents an individual mouse. *P = 0.005. (**b**) Epitope-specific T_H17 cell numbers in the brains of IL-12– or IL-23–skewed T cell recipients with either classic or atypical EAE, respectively. Differences between atypical versus classic EAE were observed only for $MOG_{79–90}$ recipients (P = 0.03). (**c**) The $\log_{10}$ T_H17:T_H1 ratios in the spleen, brain and spinal cord of F1 recipients of either IL-12– or IL-23–skewed epitope-specific T cells. Correlation of T_H17:T_H1 ratios >1 with atypical disease and <1 with classic disease was highly significant ($P = 5 \times 10^{-9}$). (**d**) Mean clinical course of T_H17-biased $MOG_{97–114}$ T cell recipients receiving either IL-17RA–Fc protein (scores are for classic EAE) or purified mouse IgG (scores are for atypical EAE). Data are pooled from two independent experiments (n = 10 mice per group). Mean clinical scores at day 6 and 7 post-transfer were significantly different (P < 0.008). Because of disease severity, control mice receiving IgG were killed at d 7. (**e**) The percentage of classic or atypical EAE observed for each group in **d**. (**f**) Representative images of brain and spinal cord sections stained with CD4 (red), F4/80 (green) and DAPI (blue). Dashed white line represents boundary between meninges and parenchyma. Scale bars, 5 μm.

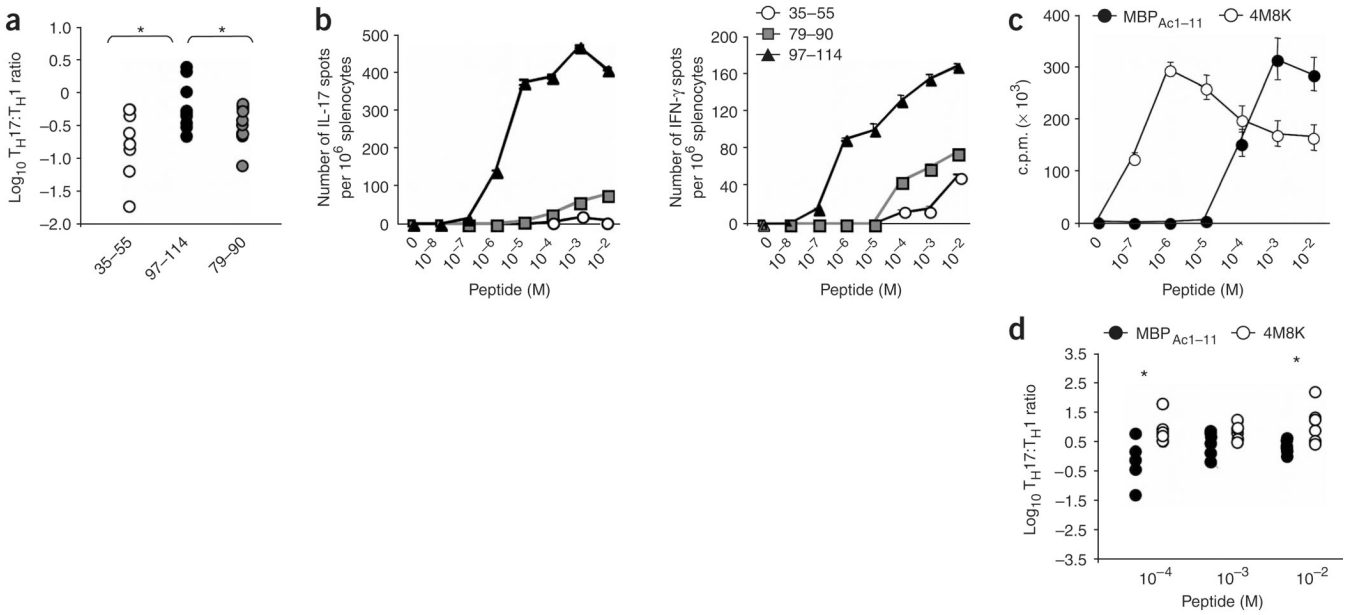

Figure 4.

T_H17:T_H1 ratio of epitope-specific T cells is influenced by functional avidity. (**a**) T_H17:T_H1 ratio of MOG-epitope specific T cells from spleens of rMOG-primed F1 mice determined by ELISPOT (each circle represents an individual mouse). (**b**) Representative dose response of rMOG-primed T cells to MOG peptides. $MOG_{97–114}$-specific T cells showed a significantly higher functional avidity compared with the other specificities ($P < 0.05$, $n = 19$ experiments). (**c**) Proliferation of $MBP_{Ac1–11}$-specific TCR transgenic T cells in response to $MBP^{Ac1–11}$ and $MBP_{Ac1–11Met4Lys8}$ peptides. (**d**) T_H17:T_H1 ratios of $MBP_{Ac1–11Met4Lys8}$- and $MBP_{Ac1–11}$-specific T cells isolated from spleens of B10.PL mice immunized with either $MBP_{Ac1–11}$ or $MBP_{Ac1–11Met4Lys8}$ were determined by ELISPOT. *$P < 0.05$. Error bars represent s.d.